Accepted Manuscript

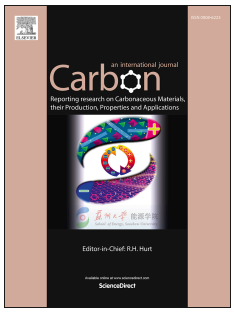

Covalent-linked porphyrin/single-walled carbon nanotube nanohybrids: Synthesis and influence of porphyrin substituents on nonlinear optical performance

Mingfei Zhang, Lulu Fu, Jun Ye, Mark G. Humphrey, Huan Liu, Bing Yan, Long Zhang, Jianda Shao, Chi Zhang

PII: S0008-6223(17)30849-7

DOI: 10.1016/j.carbon.2017.08.060

Reference: CARBON 12309

To appear in: *Carbon*

Received Date: 2 April 2017

Revised Date: 20 August 2017

Accepted Date: 26 August 2017

Please cite this article as: M. Zhang, L. Fu, J. Ye, M.G. Humphrey, H. Liu, B. Yan, L. Zhang, J. Shao, C. Zhang, Covalent-linked porphyrin/single-walled carbon nanotube nanohybrids: Synthesis and influence of porphyrin substituents on nonlinear optical performance, *Carbon* (2017), doi: 10.1016/j.carbon.2017.08.060.

Graphical Abstract:

Covalent-Linked Porphyrin/Single-Walled Carbon Nanotube Composites: Synthesis and Influence of Porphyrin Substituents on Nonlinear Optical Performance

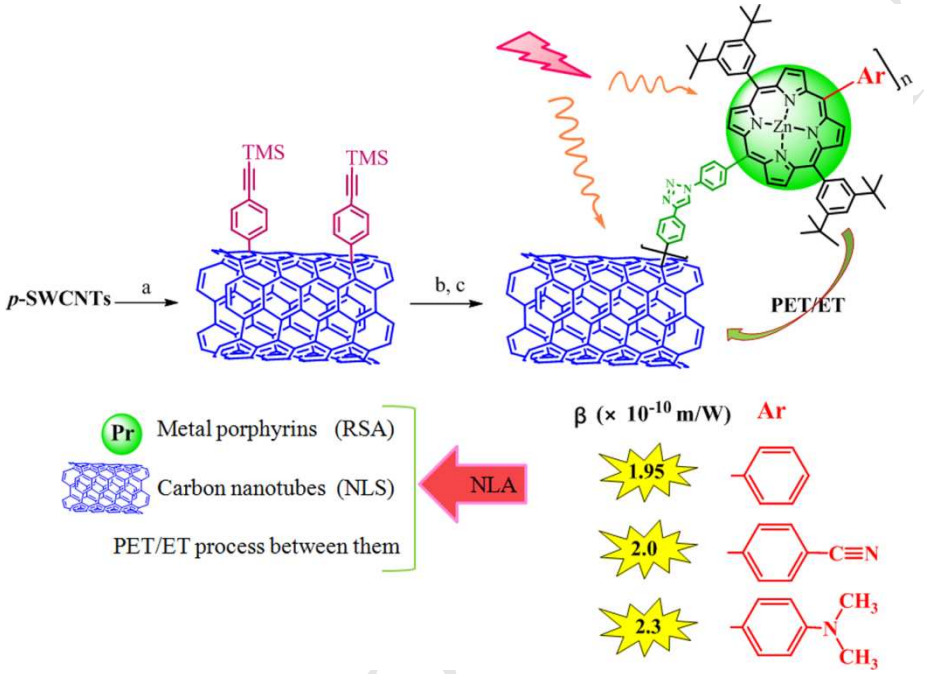

Covalent-linked porphyrin/single-walled carbon nanotube nanohybrids: synthesis and influence of porphyrin substituents on nonlinear optical performance

Mingfei Zhang [a,b,c,1], Lulu Fu [a,b,c,1], Jun Ye [a,b,*], Mark G. Humphrey [b,d], Huan Liu [a], Bing Yan [b], Long Zhang [c], Jianda Shao [c], Chi Zhang [a,b,c,*]

[a] *China-Australia Joint Research Center for Functional Molecular Materials, School of Chemical and Material Engineering, Jiangnan University, Wuxi 214122, China*

[b] *China-Australia Joint Research Center for Functional Molecular Materials, School of Chemical Science and Engineering, Tongji University, Shanghai 200092, China*

[c] *Key Laboratory of Materials for High-Power Laser, Shanghai Institute of Optics and Fine Mechanics, Chinese Academy of Sciences, Shanghai 201800, China*

[d] *Research School of Chemistry, Australian National University, Canberra, ACT 2601, Australia*

[*]Corresponding author: Tel.: +86-21-65988860; Fax: +86-21-65981097.
E-mail:, chizhang@tongji.edu.cn, czhang@siom.ac.cn

ABSTRACT

Electron-withdrawing 4-cyanophenyl-, electronically innocent phenyl-, and electron-donating 4-dimethylaminophenyl-functionalized porphyrin/single-walled carbon nanotube (SWCNT) nanohybrids have been synthesized and characterized by ultraviolet–visible absorption, steady-state fluorescence, Fourier transform infrared, and Raman spectroscopies, X-ray photoelectron spectroscopy, scanning electron microscopy, transmission electron microscopy and thermogravimetric analysis. Nonlinear optical (NLO) studies using the Z-scan technique revealed that both the cyano (CN) and the dimethylamino (DMA) substituents have a positive effect in optimizing the optical limiting performance of the SWCNT–porphyrin nanohybrids, owing to increased reverse saturable absorption (RSA) of the porphyrin moieties after functionalization by CN or DMA. In comparison with CN, the DMA group has a more positive influence on the porphyrin excited states and thereby the RSA and NLO activity.

1. Introduction

Carbon nanoallotropes from 0D to 1D and 2D, examples of which include C60, single- and multiple-walled carbon nanotubes (CNTs), and graphene, respectively, have been intensively investigated within both the scientific and the industrial communities during the past two decades [1–3]. Special attention has been paid to single-walled CNTs (SWCNTs), which comprise a single graphene layer seamlessly wrapped into a cylindrical tube with an internal void [4–8]. The hexagonal lattice of sp^2 carbon atoms bestows excellent electrical, mechanical, thermal and optical properties on SWCNTs, making them favored candidates for applications in electronic/optical devices, catalysis, and nanomedicine, and as nanoreactors [9–13]. However, owing to high surface energy and significant π-π electron interactions between the tubes, SWCNTs have a high tendency to aggregate into bundles [4]. This gives rise to very limited solubility/dispersity of SWCNTs in organic solvents or water, creating a serious difficulty for processing and thus real-life applications. To solve this, surface functionalization of SWCNTs has been proposed, which might also introduce enhanced or novel properties, thereby leading to new applications for certain functional entities (e.g. inorganics, polymers, organic dyes, etc.) [14–18].

Porphyrin is a natural organic dye comprising a square-planar 18π-electron aromatic macrocycle. It possesses many appealing properties, such as high chemical and thermal stability, a large extinction coefficient in the visible light region, multiple stable cationic states, and strong reverse saturable absorption (RSA) for laser pulses in the visible region. These attributes equip porphyrins for use across a wide range of research fields [19–22]. In addition, the rich metal coordination chemistry as well as the readily available methods of chemical modification on the periphery of the porphyrin skeleton provides great flexibility for the synthesis of novel porphyrin-dyes with specific properties [23–25].

Recently, many reports have focused on combining SWCNTs with porphyrins to form inorganic/organic hybrid composites, and this has been shown to be a promising approach in the pursuit of photon-to-electron transfer, solar energy conversion, and nonlinear optical (NLO) applications [26–29]. In particular, the combination of

porphyrins (exhibiting RSA) and SWCNTs (with strong nonlinear optical scattering (NLS) properties) results in interesting SWCNT-porphyrin (SWCNT–Pr) ns with enhanced optical limiting (OL) behavior, useful in the efficient extinction of potentially damaging high intensity light such as that from lasers [30]. The first nonlinear characterization of a SWCNT-porphyrin nanohybrid material [31], in which porphyrins spontaneously adhered to the nanotube surface in solution through non-covalent van der Waals interactions, revealed a strong nonlinear absorption effect with nanosecond pulses (Z-scan technique at 532 nm). Subsequent studies of π-π stacked SWCNT–Pr nanohybrids revealed an ultrafast OL response and a low limiting threshold from femtosecond nonlinear measurements at 780 nm [32]. In order to avoid possible dissociation and to ensure that the SWCNT–Pr nanohybrids are stable, several covalent linking methodologies have been examined [33–38]. Tian and coworkers reported that covalently-linked SWCNT–Pr has a lower linear absorption than the physically blended combination. Energy transfer (ET) and photo-induced electron transfer (PET) from porphyrins to SWCNTs play an important role in increasing the OL performance, with the π-conjugated bridge (phenylene) between the SWCNTs and the porphyrins resulting in much more efficient ET/PET than with amide or ester covalent linkages, and thereby a more efficient OL effect [30].

However, in sharp contrast to the great progress achieved in optimizing the NLO properties of purely organic porphyrins and metalloporphyrins through synthesis and modification [20,39,40], NLO research on covalently-linked SWCNT–Pr nanohybrids is sparse [34]; there is no report thus far on the influence of further chemical modification, especially at the organic porphyrin moiety, on the NLO performance of covalent SWCNT–Pr nanohybrids. In this work, we have designed and synthesized three novel SWCNTs covalently functionalized with tert-butyl substituted 5,10,15,20-tetraphenylporphyrins (TPPs), employing one classical organic electron-acceptor cyano group (CN) and one classical organic electron-donor dimethylamino group (DMA) attached at the opposite extremity of TPP to the SWCNTs (SWCNT–Pr2 and SWCNT–Pr3 respectively), as well as an example with an unmodified phenyl as control, SWCNT–Pr1 (Fig. 1). Thorough characterization

was carried out by ultraviolet-visible (UV–vis) absorption, steady-state fluorescence, Fourier transform infrared (FTIR), and Raman spectroscopies, X-ray photoelectron spectroscopy (XPS), scanning electron microscopy (SEM), transmission electron microscopy (TEM), and thermogravimetric analysis (TGA), which collectively unambiguously confirmed that the chosen porphyrins were successfully attached to the surface of the SWCNTs by a 1,2,3-triazole-containing π-conjugated covalent bridge rather than by non-covalent means. Nonlinear transmittance tests by the Z-scan technique (532 nm, 4 ns duration) revealed that both electron-withdrawing CN and electron-donating DMA substituents have positive effects in further optimizing the OL performance of the SWCNT–Pr nanohybrids, owing to the increased RSA ability of the porphyrin moieties after attaching CN or DMA. In comparison with CN, the DMA group has a more positive influence on the porphyrins' excited states and thus effectively further enhanced the RSA process and the final NLO performance of the SWCNT–Pr nanohybrids. This may provide a useful guide to the design of better NLO materials for device applications in optoelectronics and photonics.

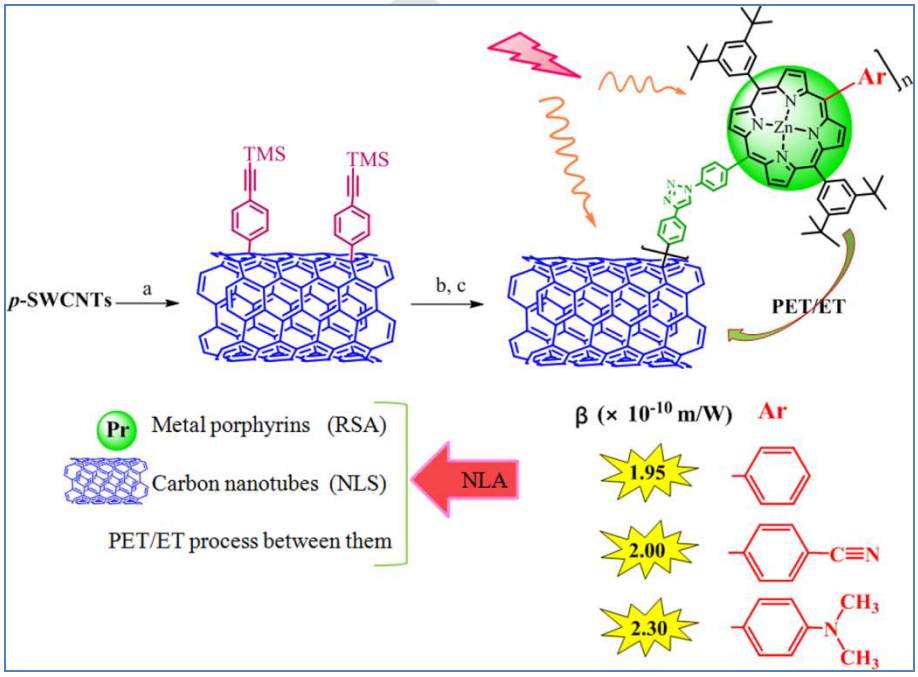

Fig. 1. Schematic depiction of the preparation and NLA origins from SWCNT–Pr1, SWCNT–Pr2 and SWCNT–Pr3. (a) 4-(2-trimethylsilyl)ethynylaniline, isoamyl nitrite, NMP, 70 °C; (b) TBAF, NMP, 0 °C; (c) Pr1 (or Pr2 or Pr3), $CuSO_4 \cdot 5H_2O$, sodium ascorbate, 70 °C.

2. Experimental

2.1 Materials and reagents

The pristine SWCNTs (*p*–SWCNTs) with average diameters of 1-2 nm and lengths of 0.5-2 μm were purchased from Beijing DK nano technology Co. Ltd. and used as received. All of the reactions were performed under a nitrogen atmosphere with the use of standard Schlenk techniques. All materials were of chemical or analytical grade. 5,15-bis-(3,5-bis{*tert*-butyl}phenyl)porphyrin 1 and 5-(4-aminophenyl)-10,20-bis-(3,5-bis{*tert*-butyl}phenyl)porphyrin 2 (Fig. 2) were prepared according to those reported literatures [41,42]. Tetrahydrofuran (THF) and diethyl ether were dried and distilled over sodium before use. *N*-methyl-2-pyrrolidone (NMP), *N*,*N*-dimethylamide (DMF), dimethylsulfoxide (DMSO), toluene, chloroform, dichloromethane (DCM), pyridine and triethylamine (TEA) were used without further purification.

2.2 Measurements

UV–visible absorption spectra (UV–vis) were recorded on TU-1901 spectrophotometer. Fluorescence spectra were obtained with a CARY Eclipse Fluorescence Spectrophotometer. FTIR spectra were recorded on a WQF-600N spectrometer. Raman spectra were measured using an inVia Raman microscope (Renishaw) with both the 532 and 785 nm lines of an Ar ion laser as excitation source. The X-ray photoelectron spectroscopy (XPS) experiments were performed on an ESCALAB250Xi system (ThermoFisher, USA) equipped with a monochromatic Al Kα (1486.6 eV) source and a concentric hemispherical energy analyser. Nuclear magnetic resonance (NMR) spectra were recorded on a Bruker (400 MHz) spectrometer using tetramethylsilane as internal standard. Mass spectral data were recorded on a Bruker Daltonics ultrafleXtreme MALDI-TOF/TOF. The water bath sonication was performed with a KQ-400KDE sonicator (400 W, 40 kHz, Kunshan Sonicator Instrument Co., Inc.). For thermogravimetric analysis (TGA), a TGA/1100SF instrument was used and samples were heated in an alumina pan in a dry nitrogen flow (20 sccm) to 600 °C at a rate of 10 °C·min^{-1}. Field emission scanning electron microscope and transmission electron microscope images were

obtained on Hitachi/S-4800 and JEM-2100 instruments, respectively. All the measurements except TGA were carried out at room temperature.

The nonlinear optical properties of the samples were investigated using the open-aperture Z-scan technique with linearly polarized 4 ns pulsed 532 nm light generated from a mode-locked Nd:YAG laser with a repetition rate of 2 Hz; the absorption extinction coefficients were calculated by the theory reported previously [43]. The normalized transmittance $T_{Norm}(z)$ as a function of position (z) is given by $T_{Norm}(z) = \text{Log}[1 + q_0(z)]/q_0(z)$, where $q_0(z) = \beta I_0 L_{eff}/[1 + (z/z_0)^2]$, $L_{eff} = [1 - \exp(-\alpha L)]/\alpha$, z_0 is the diffraction length of the beam, I_0 is the intensity of the light at focus, L_{eff} is the effective length of the sample, L is the true optical path length through the sample, and α is the linear absorption coefficient. The focal length was 400 mm. The DMF dispersions of the samples were placed in 5 mm thick quartz cells mounted on a computer-controlled translation stage, and then moved along the *z*-axis of the incident beam. The input energy and the transmitted energy were measured using two energy detectors (Rjp-765 Energy Probe), which were linked to an energy meter (Rj-7620 Energy Ratiometer, Laser Probe Inc.). A computer was used to collect and process the data that were sent from the energy meter through a GPIB interface. For the ease of comparison, all the measurements were performed at an input intensity of 0.54 J/cm^2 at room temperature, and the linear transmittance of all samples was adjusted to 68%.

2.3 Preparation of organic porphyrins

2.3.1 Preparation of 5-Bromo-15-(4-aminophenyl)-10,20-bis-(3,5-bis{tert-butyl} phenyl)porphyrin 3

N-Bromosuccinimide (NBS) (11.4 mg in 20 ml chloroform, 0.0640 mmol) was added dropwise at –14 °C to a solution of **2** (50.0 mg, 0.0640 mmol) (synthetic details see the Supporting Information, SI) and pyridine (0.3 ml) in chloroform (50 ml). The extent of the reaction was monitored by TLC. The reaction was quenched with acetone (10 ml), and the mixture was filtered and the collected solid washed with MeOH to remove residual NBS. Further purification was achieved by column chromatography (silica, 1:3 light petroleum / DCM), to give compound **3** as a purple

powder (43.0 mg, 78%). 1H NMR (400 MHz; CDCl3; SiMe4): δ = –2.90 (2H, s, 2×NH), 1.54 (36H, s, CH3), 4.02 (2H, s, NH2), 7.05 (2H, d, J = 8.0 Hz, H Ph), 7.81 (2H, t, J = 2.0 Hz, H Ph), 7.96 (2H, d, J = 8.4 Hz, H Ph), 8.06 (4H, d, J = 1.6 Hz, H Ph), 8.80–8.95 (6H, m, H β-pyrrole), 9.66 (2H, m, H β-pyrrole).

2.3.2 Preparation of 5-Phenyl-15-(4-aminophenyl)-10,20-bis-(3,5-bis{tert-butyl} phenyl)porphyrin 4

A mixture of **3** (20.0 mg, 0.0233 mmol), phenylboronic acid (3.10 mg, 0.025 mmol), tetrakis(triphenylphosphine)palladium(0) (2.70 mg, 0.00234 mmol) and potassium carbonate (32.0 mg, 0.233 mmol) was evacuated and back-filled with nitrogen 3 times. DMF/toluene (7 mL, 5:2) was added and the mixture was heated overnight at 90 °C under a nitrogen atmosphere. After cooling, the solution was filtered through silica gel. The crude product obtained after evaporating the organic solvents was further purified by column chromatography (silica, 2:3 light petroleum / DCM) to give **4** as a purple powder (16.0 mg, 80%). ^{1}H NMR (400 MHz; $CDCl_3$; $SiMe_4$): δ = –2.71 (2H, s, 2×NH), 1.54 (36H, s, CH_3), 4.00 (2H, s, NH_2), 7.05 (2H, d, *J* = 8.0 Hz, H Ph), 7.70–7.80 (5H, m, H Ph), 8.00 (2H, d, *J* = 8.4 Hz, H Ph), 8.10 (4H, d, *J* = 1.6 Hz, H Ph), 8.20–8.25 (2H, m, H Ph), 8.80–8.95 (8H, m, H β-pyrrole). MS (MALDI-TOF): *m/z* calcd for $C_{60}H_{63}N_5$ 853.51, found 853.5083 $[M]^+$.

2.3.3 Preparation of 5-(4-Cyanophenyl)-15-(4-aminophenyl)-10,20-bis-(3,5-bis {tert-butyl}phenyl)porphyrin 5

The synthetic steps followed the procedure described above for compound **4**, using 4-cyanophenylboronic acid (3.68 mg, 0.025 mmol) instead of phenylboronic acid (17.0 mg, 83%). ^{1}H NMR (400 MHz; $CDCl_3$; $SiMe_4$): δ = –2.73 (2H, s, 2×NH), 1.53 (36H, s, CH_3), 4.04 (2H, s, NH_2), 7.07 (2H, d, *J* = 8.0 Hz, H Ph), 7.81 (2H, t, *J* = 2.0 Hz, H Ph), 8.00 (2H, d, *J* = 8.4 Hz, H Ph), 8.05 (2H, d, *J* = 8.0 Hz, H Ph), 8.08 (4H, d, *J* = 1.6 Hz, H Ph), 8.35 (2H, d, *J* = 8.0 Hz, H Ph), 8.71 (2H, d, *J* = 4.8 Hz, H β-pyrrole), 8.85–9.00 (6H, m, H β-pyrrole). MS (MALDI-TOF): *m/z* calcd for $C_{61}H_{62}N_6$ 878.50, found 878.5035 $[M]^+$.

2.3.4 Preparation of 5-(4-N,N-dimethylaminophenyl)-15-(4-aminophenyl)-10,20-bis-(3,5-bis{tert-butyl}phenyl)porphyrin 6

The synthetic steps followed the procedure described above for compound **4**, using 4-(*N*,*N*-dimethyl)phenylboronic acid (4.13 mg, 0.025 mmol) instead of phenylboronic acid (14.6 mg, 70%). ^{1}H NMR (400 MHz; $CDCl_3$; $SiMe_4$): δ = –2.67 (2H, s, 2×NH), 1.53 (36H, s, CH_3), 3.23 (6H, s, CH_3), 4.03 (2H, s, NH_2), 7.06 (2H, d, *J* = 8.4 Hz, H Ph), 7.11 (2H, d, *J* = 8.8 Hz, H Ph), 7.79 (2H, t, *J* = 2.0 Hz, H Ph), 8.00 (2H, d, *J* = 8.4 Hz, H Ph), 8.10 (6H, m, H Ph), 8.80–8.95 (8H, m, H β-pyrrole). MS (MALDI-TOF): *m/z* calcd for $C_{62}H_{68}N_6$ 896.55, found 896.5505 $[M]^+$.

2.3.5 Preparation of [5-Phenyl-15-(4-triazinophenyl)-10,20-bis-(3,5-bis{tert-butyl} phenyl)porphinato]zinc(II) Pr1

To a solution of **4** (50.0 mg, 0.0585 mmol) in THF/water (10 mL, 9:1) at 0 °C were added hydrochloric acid (0.3 ml, 10%) and sodium nitrite (4.40 mg in 0.5 ml water, 0.0638 mmol). After stirring for 10 min, two portions of sodium azide (each 4.20 mg in 0.2 ml water, 0.0646 mmol) were added dropwise with an interval time of 30 min. The reaction was completed within 2 h and the mixture was then extracted with CH_2Cl_2. Flash column chromatography using CH_2Cl_2 as eluent afforded a purple solid which was then directly used for the next step without further purification. The solid was stirred with $Zn(OAc)_2{\cdot}2H_2O$ (100 mg, 0.457 mmol) in CH_2Cl_2 / CH_3OH (8:1, 100 ml) at room temperature for 24 h in the absence of light. The crude product was purified by column chromatography (silica, 3:1 light petroleum / DCM) to give **Pr 1** as a purple powder (38.1 mg, 72%). ^{1}H NMR (400 MHz; $CDCl_3$; $SiMe_4$): δ = 1.53 (36H, s, CH_3), 7.40 (2H, d, *J* = 8.0 Hz, H Ph), 7.70–7.85 (5H, m, H Ph), 8.12 (4H, s, H Ph), 8.23 (4H, t, *J* = 6.4 Hz H Ph), 8.95 (4H, m, H β-pyrrole), 9.02 (4H, m, H β-pyrrole). MS (MALDI-TOF): *m/z* calcd for $C_{60}H_{59}N_7Zn$ 941.41, found 941.4123 $[M]^+$.

2.3.6 Preparation of [5-(4-Cyanophenyl)-15-(4-triazinophenyl)-10,20-bis-(3,5-bis {tert-butyl}phenyl)porphinato]zinc(II) Pr2

The synthetic steps followed the procedure described above for compound **Pr 1**, using **5** (50.0 mg, 0.0569 mmol) as the starting reactant instead of **4** (42.9 mg, 78%). ^{1}H NMR (400 MHz; $CDCl_3$; $SiMe_4$): δ = 1.53 (36H, s, CH_3), 7.39 (2H, d, *J* = 8.4 Hz, H Ph), 7.82 (2H, t, *J* = 2.0 Hz, H Ph), 8.05 (2H, d, *J* = 8.4 Hz, H Ph), 8.09 (4H, d, *J* =

1.6 Hz, H Ph), 8.20 (2H, d, *J* = 8.4 Hz, H Ph), 8.35 (2H, d, *J* = 8.4 Hz, H Ph), 8.83 (2H, d, *J* = 4.8 Hz, H β-pyrrole), 8.95 (2H, d, *J* = 4.4 Hz, H β-pyrrole), 9.03 (4H, m, H β-pyrrole). MS (MALDI-TOF): *m/z* calcd for $C_{61}H_{58}N_8Zn$ 966.41, found 966.4075 $[M]^+$.

2.3.7 Preparation of [5-(4-N,N-dimethylaminophenyl)-15-(4-triazinophenyl)-10,20-bis-(3,5-bis{tert-butyl}phenyl)porphinato]zinc(II) Pr3

The synthetic steps followed the procedure described above for compound **Pr1**, using **6** (50.0 mg, 0.0528 mmol) as the starting reactant instead of **4** (35.5 mg, 65%). ^{1}H NMR (400 MHz; $CDCl_3$; $SiMe_4$): δ = 1.53 (36H, s, CH_3), 3.00 (6H, s, $N(CH_3)_2$), 7.39 (2H, d, *J* = 8.4 Hz, H Ph), 7.53 (2H, d, *J* = 8.8 Hz, H Ph), 7.79 (2H, t, *J* = 2.0 Hz, H Ph), 8.04 (2H, d, *J* = 8.0 Hz, H Ph), 8.09 (4H, d, *J* = 1.6 Hz, H Ph), 8.21 (2H, d, *J* = 8.0 Hz, H Ph), 8.91 (2H, d, *J* = 4.8 Hz, H β-pyrrole) , 8.95–9.05 (4H, m, H β-pyrrole), 9.04 (2H, m, H β-pyrrole). MS (MALDI-TOF): *m/z* calcd for $C_{62}H_{64}N_8Zn$ 984.45, found 984.4545 $[M]^+$.

2.4 Preparation of f–SWCNTs

A mixture of *p*–SWCNTs (15 mg) and NMP (50 mL) was sonicated for 30 min, and then 2.5 equiv. C of 4-(2-trimethylsilyl)ethynylaniline (594 mg, 3.14 mmol) and 28 equiv. C of isoamyl nitrite (426 μL, 3.17 mmol) were added. The resultant suspension was stirred at 70 °C for three days under a nitrogen atmosphere before another identical portion of 4-(2-trimethylsilyl)ethynylaniline and isoamyl nitrite was added. After another four days, the suspension was filtered through a PTFE membrane (0.22 μm), and the collected solid washed several times with NMP and CH_2Cl_2. The resulting filter cake was redispersed in NMP (50 mL). The entire filtering procedure above was repeated several times until the mass of the filter cake were constant, giving a black powder of 18 mg. FTIR: ν (cm^{-1}) = 2931, 2877, 1108.

2.5 Preparation of SWCNT–Pr1, SWCNT–Pr2, SWCNT–Pr3

All the novel nanohybrids were prepared according to the following procedure: A mixture of *f*–SWCNTs (10.0 mg) and NMP (40 mL) was sonicated for 30 min after which tetra-*n*-butylammonium fluoride (1.40 g) was added at 0 °C. The reaction was completed after stirring at room temperature for 2 h. The suspension was then filtered

through a PTFE membrane (0.22 μm) and the collected solid washed several times with DMF, THF and CH_2Cl_2. The entire filtering procedure above was repeated several times until the mass of the filter cake was constant. It was then immediately redissolved in NMP (20 ml), and Pr1 (15 mg) (or Pr2 or Pr3) (synthetic details see the SI), $CuSO_4{\cdot}5H_2O$ (3.20 mg, 0.0128 mmol), and sodium ascorbate (24.8 mg, 0.125 mmol) were added successively. The reaction mixture was stirred at 70 °C for 48 h and then cooled to room temperature. In order to thoroughly remove residues including sodium ascorbate, copper catalyst and unbound ZnP, the resultant mixture was resonicated and washed successively with mixtures of DMF/water (v/v = 1/2) and DMF/THF (v/v = 1/2). These operations were repeated several times and the filter cakes were further washed with THF and CH_2Cl_2. The yields of the final dried products SWCNT–Pr1, SWCNT–Pr2 and SWCNT–Pr3 were 15, 15, and 16 mg, respectively.

3. Results and Discussion

3.1 Synthesis

To introduce additional electronically active organic groups onto traditional SWCNT–Pr nanohybrids, we used a synthetic strategy to build differently substituted porphyrins in advance of linking them onto SWCNTs through the azide-alkyne click reaction. The successful preparation of porphyryl azides with different substituents is therefore a key component of the overall synthesis (Fig. 2). To this end, 5,15-bis-(3,5-bis{*tert*-butyl}phenyl)porphyrin **1** was first obtained by acid catalyzed condensation of 3,5-bis{*tert*-butyl}benzaldehyde and dipyrrolylmethane [41]. A nucleophilic attack at one of the free meso-carbons of **1** was then carried out by Senge's method [42], using an organolithium reagent freshly prepared by treating 4-bromoaniline with 3 molar equivalents of *n*-butyllithium, and subsequent oxidation with 2,3-dicyano-5,6-dichlorobenzoquinone (DDQ) to afford compound **2**. Bromination at the last free meso position of **2** with *N*-Bromosuccinimide (NBS) [44] then afforded **3**. Suzuki-Miyaura cross-coupling of **3** and the different three aryl boronic acids gave compounds **4**, **5**, and **6**, differentiated by H, CN, and NMe_2

substituents, respectively. Porphyryl azides were then synthesized from the corresponding porphyryl amines via their diazonium compounds, and these were subsequently metalated by zinc in order to avoid possible copper insertion during the final Cu(II)-catalyzed click reaction step. All the aforementioned reactions proceeded in moderate to high yields (48–78%).

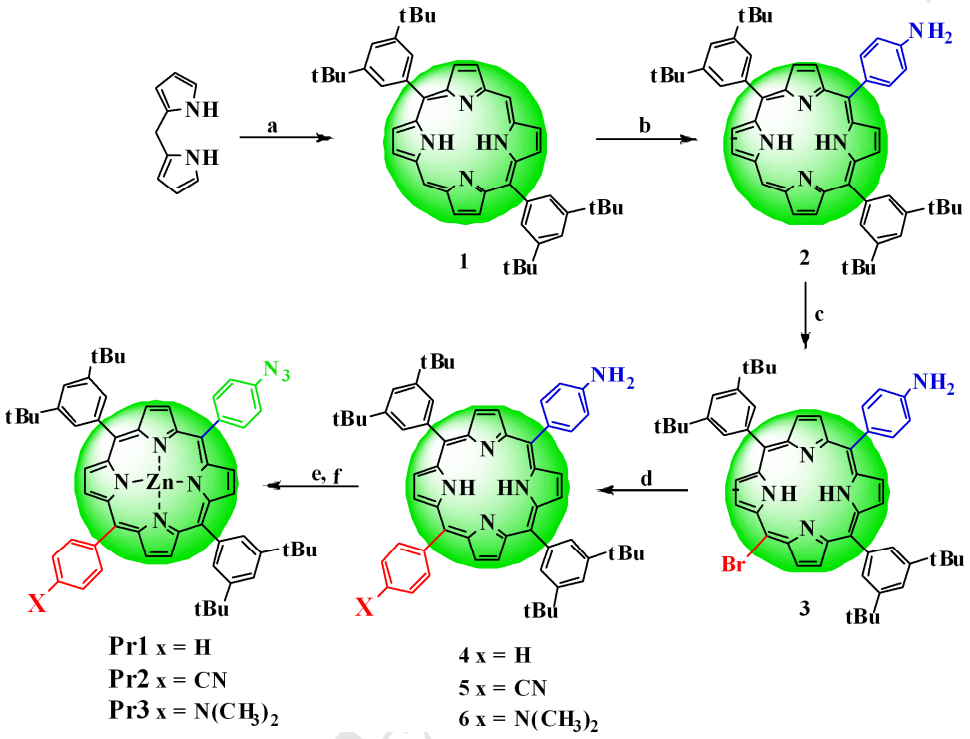

Fig. 2. Synthesis of Pr1, Pr2 and Pr3. (a) 3,5-di(*tert*-butyl)benzaldehyde, TFA, DDQ, Et_3N, CH_2Cl_2, RT; (b) 4-bromoaniline, *n*-BuLi, Et_2O, 0 °C to RT; (c) NBS, pyridine, CH_2Cl_2, –14 °C; (d) arylboronic acid (phenylboronic acid, 4-cyanophenylboronic acid, or 4-(*N*,*N*-dimethyl)phenylboronic acid), $Pd(PPh_3)_4$, K_2CO_3, DMF/toluene, 90 °C; (e) $NaNO_2$, HCl, NaN_3, 0 °C; (f) $Zn(OAc)_2 2H_2O$, MeOH/CH_2Cl_2, RT.

The *p*–SWCNTs were initially covalently grafted with trimethylsilyl-protected ethynylphenylene groups, forming *f*–SWCNTs (Fig. 1). After removal of the protecting trimethylsilyl group, these pre-functionalized SWCNTs were immediately mixed with the porphyryl azides to yield the final SWCNT–Pr1, SWCNT–Pr2 and SWCNT–Pr3 by azide-alkyne cycloadditions. After purification, all functionalized SWCNTs were found to have increased in weight by ca. 50% during this final step. After a few minutes of ultrasonic treatment, all of the as-prepared nanohybrid materials exhibit a green-grey color and significantly improved stability in

dimethylsulfoxide (DMSO), dimethylpyrrolidone (NMP), and dimethylformamide (DMF), and are stable for several weeks at room temperature, while dispersions of the *p*–SWCNTs in DMF show a gray color and quickly agglomerate (Fig. 3).

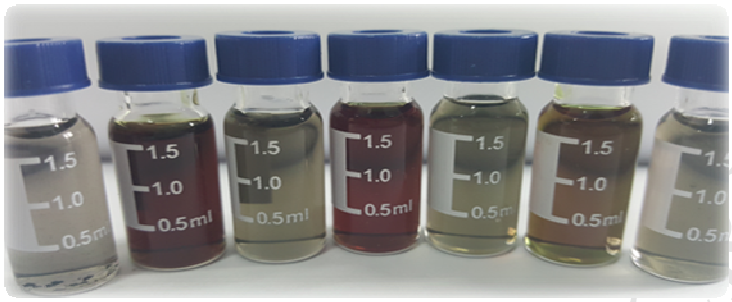

Fig. 3. Photograph of the samples dispersed in DMF (from left to right: *p*–SWCNTs, Pr1, SWCNT–Pr1, Pr2, SWCNT–Pr2, Pr3 and SWCNT–Pr3).

3.2 UV–vis and Fluorescence spectroscopy

The UV–vis absorption spectra of *p*–SWCNTs, Prs and SWCNT–Prs in DMF are displayed in Fig. 4 and the key data summarized in Table 1. The UV–vis spectrum of *p*–SWCNTs contains a typical broad absorption peak at ca. 300 nm with the intensity slowly decreasing on proceeding to longer wavelengths [45]. The porphyrins with varying substituents (H, CN, DMA) opposite to the azide group (Fig. 2) show strong Soret absorptions at ca. 430 nm and weak Q bands at ca. 560 and 600 nm. There was little spectral change seen on proceeding from Pr1 to the CN-substituted Pr2, while the DMA-containing Pr3 exhibits slightly red-shifted but much broadened Soret and Q bands when compared to Pr1 (Soret, 428 nm to 430 nm; Q, 560/601 nm to 565/607 nm). The absorption profile of these SWCNT–Pr nanohybrids combine the spectral characteristics of both the *p*–SWCNTs and the corresponding porphyrins, except for a distinct 2-3 nm red shift of the porphyrin signals, the latter suggestive of a successful covalent combination of the SWCNTs and the porphyrins. It is also noteworthy that the differences in the Soret and Q bands of SWCNT–Pr1, 2, and 3 mimic those observed for the Pr1, 2 and 3 precursors, i.e. SWCNT–Pr3 with electron-donating DMA substituents possesses broader and slightly red-shifted Soret and Q bands compared to SWCNT–Pr1 and SWCNT–Pr2. This suggests that DMA promotes

electronic communication within the molecule or the composite systems in the ground states, an outcome of its classical electron-donating nature.

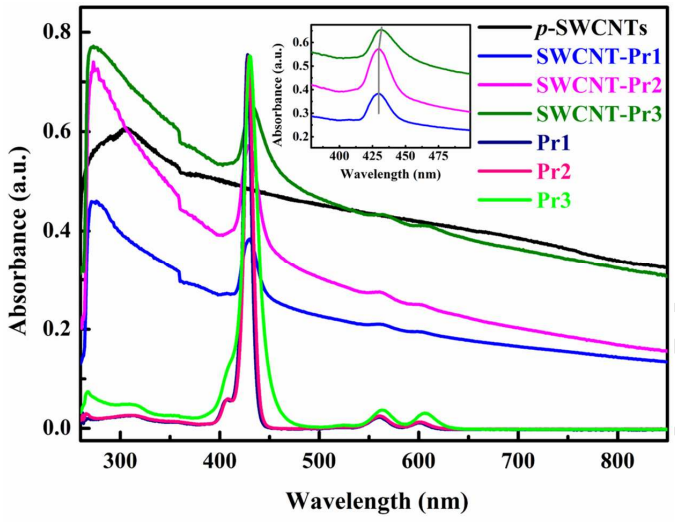

Fig. 4. UV–vis absorption spectra of *p*–SWCNTs, Pr1, Pr2 and Pr3, SWCNT–Pr1, SWCNT–Pr2 and SWCNT–Pr3. Inset: spectra of SWCNT–Pr1, SWCNT–Pr2 and SWCNT–Pr3 within the range 375-500 nm.

Table 1. Absorption and emission spectra parameters (λ_{abs} and λ_{em}) of Pr1, Pr2, Pr3, SWCNT–Pr1, SWCNT–Pr2 and SWCNT–Pr3.

Samples	λ_{abs} (Q_2) /nm	λ_{abs} (Q_1) /nm	Soret/nm	λ_{em2}/nm	λ_{em1}/nm
Pr1	601	560	428	660	608
SWCNT–Pr1	604	563	430	660	608
Pr2	601	560	429	663	611
SWCNT–Pr2	603	562	431	663	612
Pr3	607	565	430	–	623
SWCNT–Pr3	609	566	433	–	623

To probe the excited-state interactions in these composites, we carried out fluorescence spectra measurements in DMF, exciting at 430 nm, and with the porphyrin absorption intensities adjusted to be identical. Fig. 5 illustrates the fluorescent emissions of *p*–SWCNTs, Prs and SWCNT–Prs. *p*–SWCNTs failed to exhibit any noticeable emissions in the 550-750 nm region. In this region, two characteristic porphyrin photoluminescence bands emitting from the singlet excited states of S_1 and S_2 were observed, with the S_1-S_0 transitions showing luminescence maxima. The differences in fluorescence amongst the Prs are much more prominent than differences in their absorption profiles. The introduction of CN in Pr2 gives rise

to a bathochromic shift in the emission peaks of ca. 3 nm and with a slightly decreased intensity, while DMA in Pr3 intensifies the emissions and red-shifts the S_1 fluorescence by 15 nm, resulting in mixing with the S_2 fluorescence. These behaviors should be correlated with the inductive electron effect and/or conjugation effect of the CN and DMA group; DMA in particular should enhance the intramolecular charge transfer (ICT) from porphyrin through the azide group by enhancing the electron density at the porphyrin [46,47]. Interestingly, the fluorescence profiles and wavelengths of each SWCNT–Pr nanohybrid is almost identical with those of its corresponding Pr (Fig. 5 and Table 1), which suggests that the singlet excited states of the composites are mostly located on the porphyrins and their peripheral organic substituents, rather than the SWCNTs. Nevertheless, the SWCNTs still played a key role in quenching the S_1 and S_2 excitons (Fig. 1); as a result, the fluorescence intensity was quenched by 97%/98%/99% in SWCNT–Pr1/SWCNT–Pr2/SWCNT–Pr3, respectively, demonstrating efficient ET/PET from porphyrins to the carbon nanotubes [48,49].

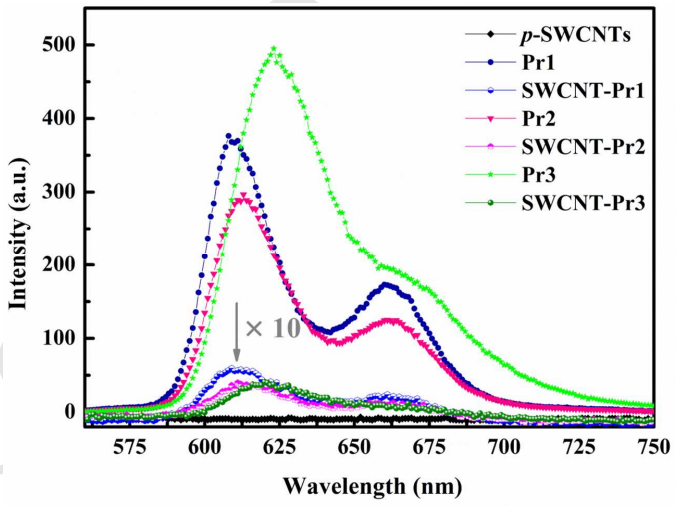

Fig. 5. Fluorescence spectra of Pr1, Pr2, Pr3, SWCNT–Pr1, SWCNT–Pr2 and SWCNT–Pr3 in DMF upon excitation at 430 nm (ten times magnification of the fluorescence curves of *p*–SWCNTs, SWCNT–Pr1, SWCNT–Pr2 and SWCNT–Pr3).

3.3 FTIR, Raman and X-ray photoelectron spectroscopy

FTIR, Raman and X-ray photoelectron spectroscopy can be used to track the stepwise conversion from *p*–SWCNTs to terminal porphyrin-covalently

functionalized SWCNTs. FTIR spectra of *p*–SWCNTs, *f*–SWCNTs, Prs, and SWCNT–Prs are compared in Fig. 6. In the spectrum of *p*–SWCNTs, no obvious signals are observed, indicating that nothing is on the surface of the as-received *p*–SWCNTs. Following treatment with 4-trimethylsilylethynylaniline diazonium compounds, new broad peaks at 2933 and 2885 cm^{-1} corresponding to the C–H vibrations of the trimethylsilyl group are observed in the spectra of *f*–SWCNTs, which suggests an initial covalent attachment onto the surface of the SWCNTs. After removal of the protecting trimethylsilyl group and subsequent azide-alkyne cycloaddition with the porphyrin azides, the FTIR spectra are modified significantly. The characteristic signals of the trimethylsilyl groups and the strong absorption at ca. 2120 cm^{-1} from the azide unit of Prs disappear [50], while several fingerprint peaks appear in the FTIR spectra of the composites, including sharp bands at 2850, 2922 and 2957 cm^{-1} of the C–H stretching modes, 1715 cm^{-1} corresponding to the bending vibration of the C=N bonds from the porphyrin skeletons [51], and a characteristic signal at 1015 and 1057 cm^{-1} from the newly formed triazole rings [52–54]. These spectroscopic changes are consistent with the successful covalent functionalization of the SWCNTs with porphyrins via the green and efficient “click” reaction.

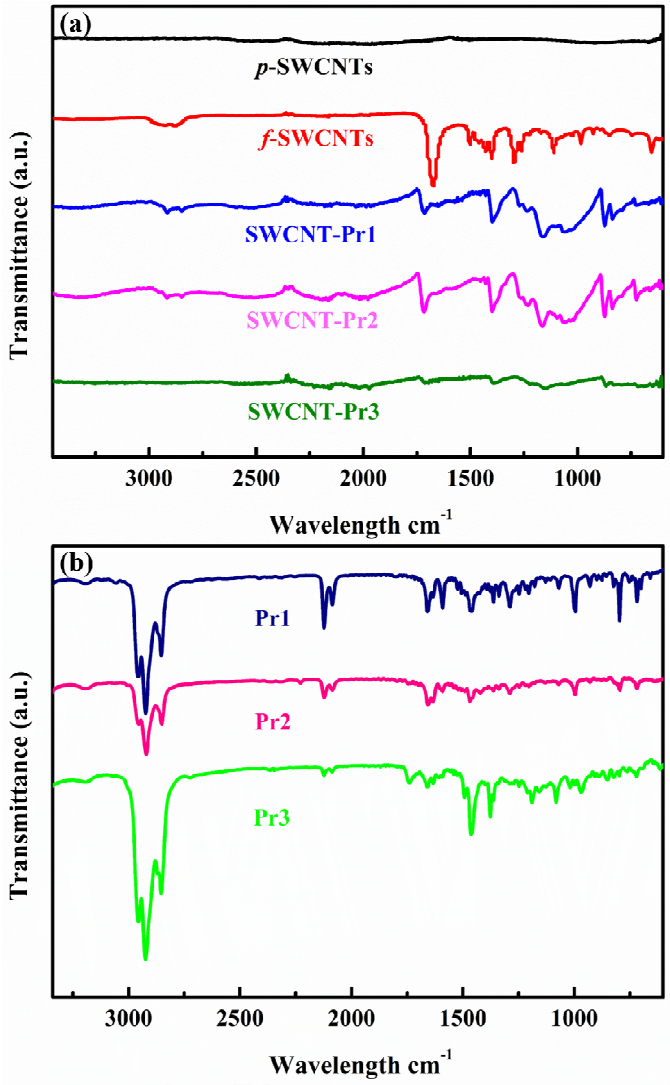

Fig. 6. FTIR spectra of (a) *p*–SWCNTs, *f*–SWCNTs, SWCNT–Pr1, SWCNT–Pr2 and SWCNT–Pr3 and (b) Pr1, Pr2, and Pr3.

This conclusion is also supported by Raman spectroscopy, and specifically changes in the D and G bands (Fig. 7), which correspond to sp^3- and sp^2-hybridized carbons of the carbon nanotubes, respectively [55,56]. Proceeding from *p*–SWCNTs to *f*–SWCNTs results in the G band shifting to slightly lower frequencies and the intensity ratio of the D band to the G band (I_D/I_G) increasing under both 532 nm (1.06 to 1.15) and 785 nm (1.87 to 1.96) laser excitation. This provides strong evidence for the transformation of sp^2 carbons into sp^3 carbons within the SWCNT framework, and thus effective covalent chemical modification of the SWNCT surface [57–59]. When *f*–SWCNTs are further transformed to SWCNT–Prs, the I_D/I_G ratio is invariant under

785 nm excitation (1.96 to 1.97, 1.95, and 1.96 for SWCNT–Pr1, SWCNT–Pr2, and SWCNT–Pr3, respectively), but decreases under 532 nm radiation (1.15 to 1.01, 1.02, and 1.05 for SWCNT–Pr1, SWCNT–Pr2, and SWCNT–Pr3, respectively). This difference can be understood as follows: with 532 nm excitation, porphyrins have non-negligible Raman signals between 1400 and 1600 cm^{-1} (Fig. S1 in the SI), which overlap the D band of SWCNTs near 1600 cm^{-1}, and thus afford a misleading result of decreased I_D/I_G ratios, while in contrast, 785 nm excitation results in no observable Raman signals for porphyrins in the wavelength regions of interest (Fig. S2 in the SI). The nearly constant I_D/I_G ratios of *f*–SWCNTs and SWCNT–Pr1-3 with 785 nm laser excitation are therefore more reliable, and consistent with the "click" reaction step taking place at the pendant acetylenes on the SWCNTs rather than directly on the SWCNT sidewalls [60,61].

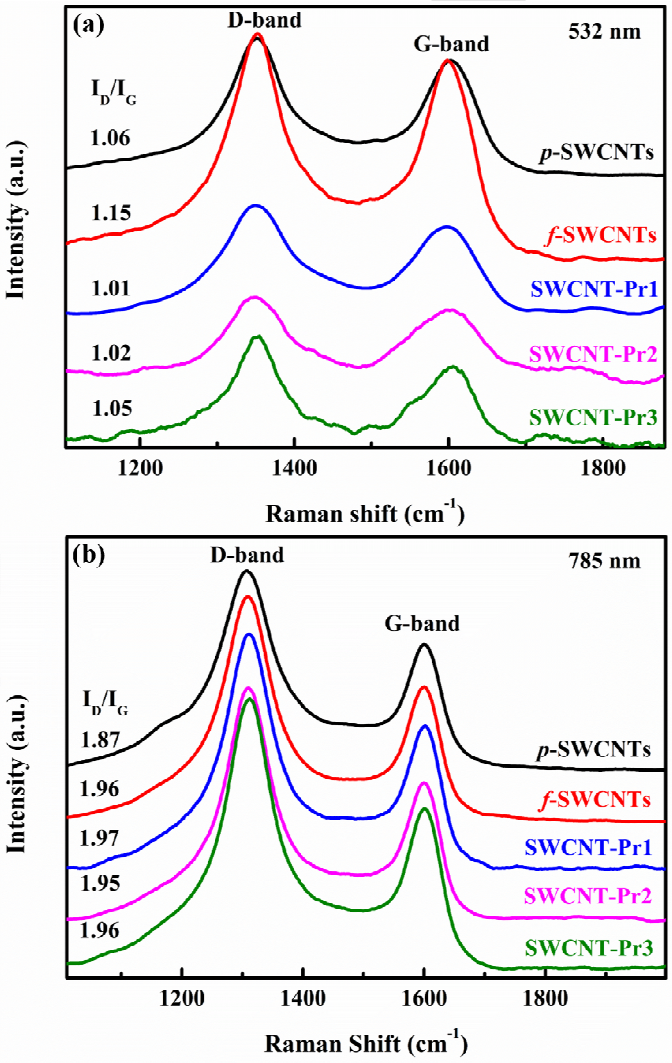

Fig. 7. Raman spectra of *p*–SWCNTs, *f*–SWCNTs, SWCNT–Pr1, SWCNT–Pr2 and SWCNT–Pr3 at different excitation wavelengths: (a) 532 nm and (b) 785 nm.

XPS is a unique surface analysis technique that may determine relative atomic composition, in the present case providing evidence of the covalent attachment of the porphyrin moieties onto the surface of the SWCNT. From Fig. 8a, four main peaks, corresponding to the carbon, nitrogen, fluorine (tetra-*n*-butylammonium fluoride residual) and zinc species are observed in the spectra of SWCNT–Pr1, SWCNT–Pr2, SWCNT–Pr3, while only carbon, oxygen species were found in the unfunctionalized *p*–SWCNT. Moreover, two additional peaks can be unambiguously observed in SWCNT–Pr1, SWCNT–Pr2, SWCNT–Pr3 that are ascribed to Zn $2p_{1/2}$ at 1044.0 eV and Zn $2p_{3/2}$ at 1021.0 eV respectively (Fig.8e: Zn 2p spectrum of SWCNT-Pr3, Zn 2p spectra of SWCNT–Pr1, SWCNT–Pr2 see Fig. S3 in SI). These XPS spectra confirm the successfully covalent attachment of ZnTPPs to carbon nanotubes. The expanded N 1s regions of three nanohybrids (Figs. 8b, 8c, 8d) reveal different peaks owing to structural difference. A single N 1s peak is observed at a binding energy of 398.3 eV, arising from the four nitrogen atoms of the metalloporphyrin macrocycle [62,63]. This peak proves the presence of ZnTPPs in the nanotube derivatives. Another N 1s peak located at ca. 402.0 eV is attributed to one of the nitrogen atoms of the triazole ring [62,64], which is a powerful proof that azidoporphyrins are covalently attached to the nanotube surface via a triazole ring and click reaction and are not simply physisorbed on the surface by π-stacking interaction.

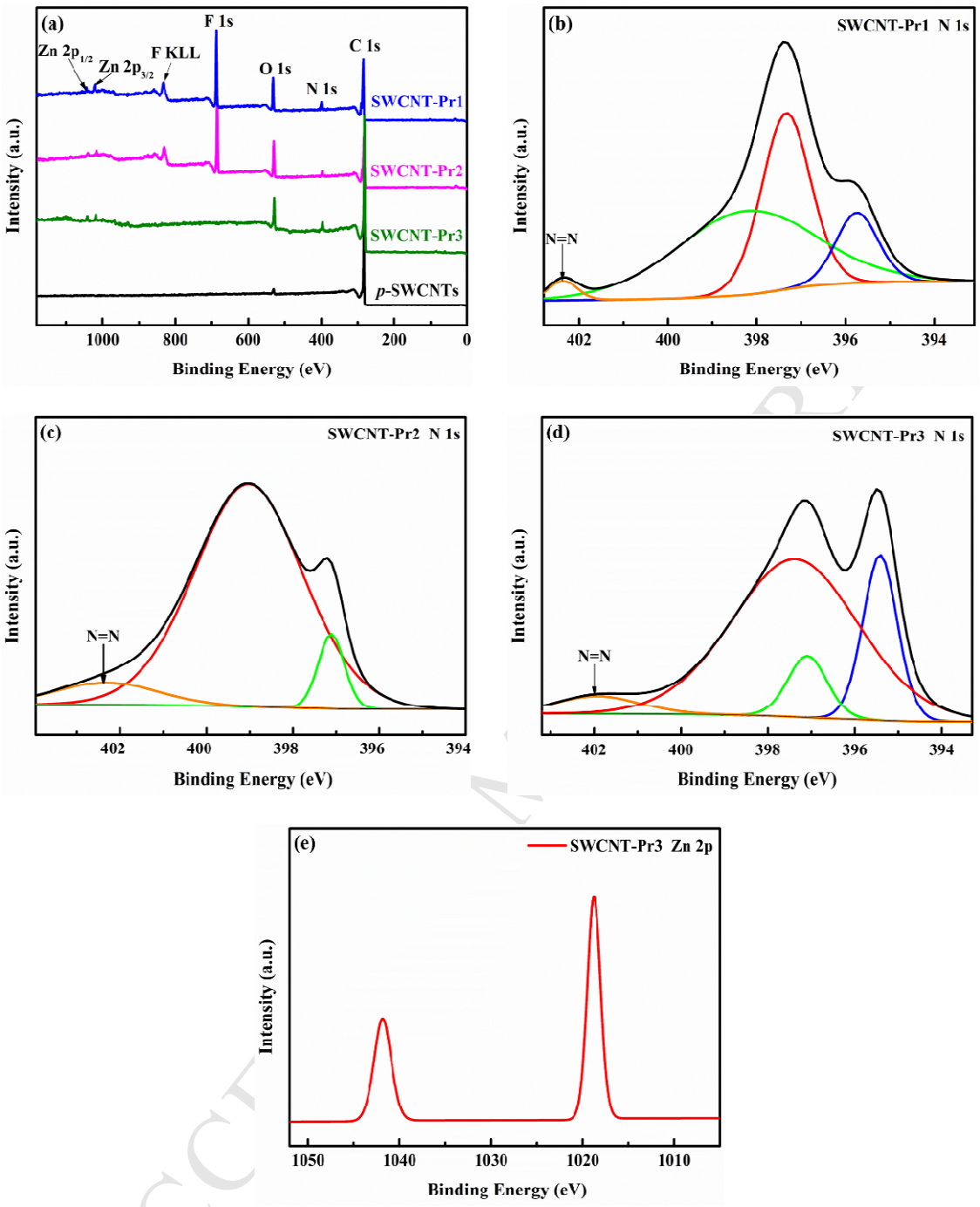

Fig. 8. (a) XPS survey spectra of *p*–SWCNTs, SWCNT–Pr1, SWCNT–Pr2 and SWCNT–Pr3; (b) N 1s XPS spectrum of SWCNT–Pr1; (c) N 1s XPS spectrum of SWCNT–Pr2; (d) N 1s XPS spectrum of SWCNT–Pr3; (e) XPS spectrum of SWCNT–Pr3 in the regions of Zn $2p_{1/2}$ and Zn $2p_{3/2}$.

3.4 Morphological analysis

The morphological features of the *p*–SWCNTs and the as-prepared SWCNT–Pr nanohybrids were investigated by SEM and TEM. These techniques confirmed the

existence of individual as well as very thin bundles of SWCNTs. As shown in the SEM and TEM images (Fig. 9), the surface of the *p*–SWCNTs is smooth and clean without any species adhering to the nanotubes. In contrast, discontinuous and irregular nanoparticles were observed on the surfaces of the SWCNT–Prs. Although information obtained from SEM and TEM should not be over-interpreted, these electron microscope techniques do provide complementary evidence for the covalent functionalization of SWCNTs with porphyrins [65,66].

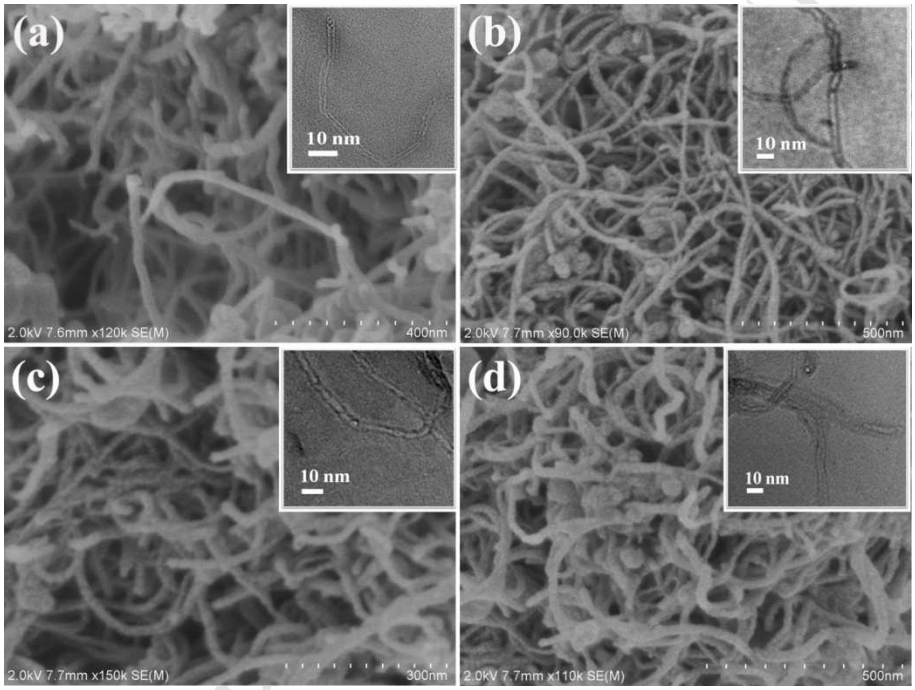

Fig. 9. SEM and TEM (inset) images of (a) *p*–SWCNTs, (b) SWCNT–Pr1, (c) SWCNT–Pr2 and (d) SWCNT–Pr3.

3.5 Thermogravimetric analysis

Thermogravimetric analysis (TGA) has been employed widely to authenticate the thermodynamic stabilities of carbon nanoallotropes [67–69]. The thermodynamic stabilities of the *p*–SWCNTs, *f*–SWCNTs and SWCNT–Prs were investigated by TGA under a nitrogen atmosphere flow (Fig. 10). The TGA curve of *p*–SWCNTs reveals no loss of weight upon increasing the temperature from 25 to 600 °C, which indicates little residual amorphous carbon remaining and no organic or inorganic impurities trapped in the *p*–SWCNTs. However, *f*–SWCNTs showed an obvious thermodynamic

instability with approximately 15% weight loss in the temperature range 25–600 °C. This weight loss corresponds to the loss of the (2-trimethylsilyl)ethynylphenyl moieties, which were covalently bound to the surface of the SWCNTs. Over the same temperature range of 25–600 °C, poorer thermodynamic stability was observed for SWCNT–Prs, and approximately 45–50% weight loss was seen, with ca. 30–35% of the net weight loss. According to the reported literatures [34,70-72], large weight loss of pure porphyrins was found at 450 to 550 □, from which it could be inferred that the sudden and abrupt decrease arises mainly from the dissociation of covalently bound TPP moieties, but to different degrees. At the same time, this TGA result could be used as another proof to authenticate that the porphyrin moieties were successfully introduced to the surface of SWCNTs.

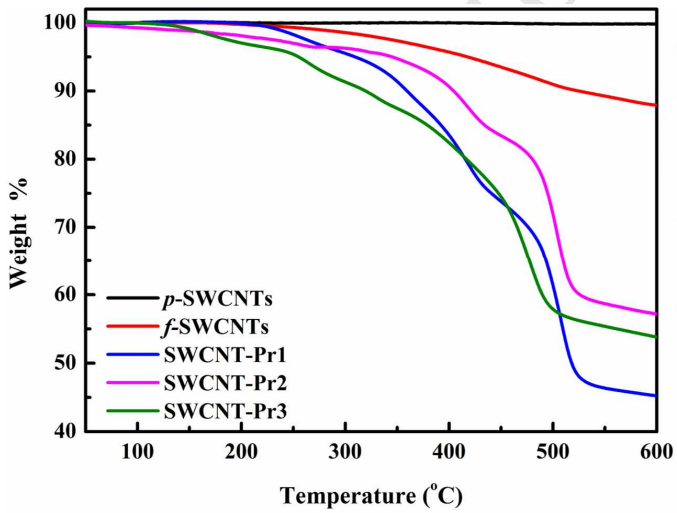

Fig. 10. TGA thermograms of *p*–SWCNTs, *f*–SWCNTs, SWCNT–Pr1, SWCNT–Pr2 and SWCNT–Pr3 at a heating rate of 10 °C·min^{-1} under a nitrogen atmosphere.

3.6 Nonlinear optical properties

Previous works has confirmed that enhanced third-order NLO performance can be achieved by hybridizing SWCNTs and porphyrins both covalently and non-covalently [31–35]. In contrast, reports exploring the impact of further chemical modification at the organic porphyrin moiety on the third-order NLO performance of composite materials are lacking. Seeking to bridge this gap in our understanding, the nonlinear transmittance of the three TPP derivatives differing in one meso terminal

substituent (H, CN, DMA) as well as their corresponding SWCNT-based nanohybrids that contain similar weight ratios of porphyrins were investigated by the open-aperture Z-scan technique using linearly polarized 4 ns duration laser pulses at 532 nm. The blank solvent DMF was also measured under the same conditions and no NLO response was found (Fig. S4 in the SI). This gives assurance that any detectable NLO responses stem from the novel materials prepared in this work. The experimental data points and their theoretical fits (solid lines) are shown in Fig. 11.

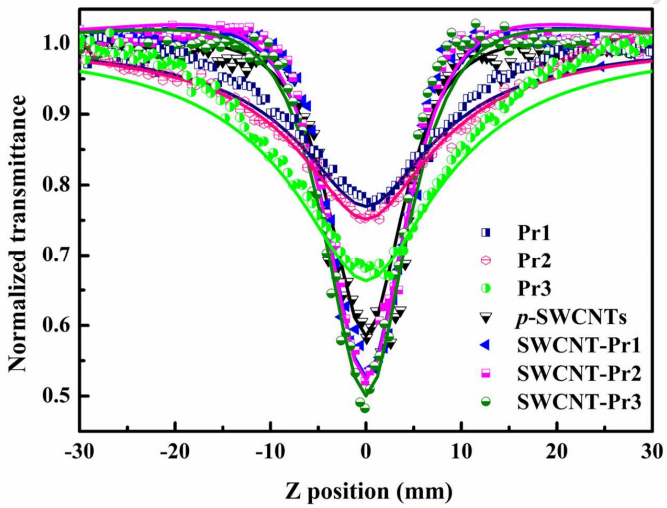

Fig. 11. Normalized open-aperture Z-scan data of Pr1, Pr2, Pr3, *p*–SWCNTs, SWCNT–Pr1, SWCNT–Pr2, and SWCNT–Pr3 at a wavelength of 532 nm in the 4-ns regime. The solid lines are the numerical fittings.

All samples exhibited a distinct reduction in transmittance when they approached the focus of the 532nm laser beam, indicative of their excellent OL effect, a property that can be employed for the protection of eyes or optical sensors [31,32]. At the focal point (Z = 0), the light transmittance (T) of Pr1, Pr 2, Pr3, and *p*–SWCNTs is reduced to 77%, 75%, 67%, and 58%, respectively, and that of SWCNT–Pr1, SWCNT–Pr2, and SWCNT–Pr3 is reduced further to 54%, 52%, and 47%, respectively, from their initial normalized settings. The hybrid composites based on SWCNTs and porphyrins therefore demonstrate superior optical limiting behavior to that of their individual constituents, either SWCNTs or porphyrins, an observation in agreement with previous reports [31–35,56,59]. Both the CN (in Pr2 and SWCNT–Pr2) and DMA (in

Pr3 and SWCNT–Pr3) substituents have a positive effect on the OL performance compared to the behavior of the reference samples Pr1 and SWCNT–Pr1. In particular, the simple classical electron-donor group DMA affords the best OL effect among the Prs and composites, which is possibly owing to the fact that DMA can stabilize holes effectively after the excitation. As for the electron-withdrawing group CN, on the one hand, the relatively stable triple bond within the CN group may give rise to the conjugation enlargement of porphyrin [73,74], generating positive effect on NLO performance of porphyrin and its corresponding hybrid [75]. On the other hand, it is also known that CN group possesses limited influence on the intramolecular charge transfer between the CN group and the macrocycle of porphyrin, which may lead to a weakly changed HOMO–LUMO gap and a small modification on the photophysical properties of Pr2 and its nanohybrid SWCNT-Pr2 [76]. Owing to the joint effect from the aforementioned two reasons, the CN group will possess a weak improvement on the NLO performance of Pr2 and its nanohybrid SWCNT-Pr2, particularly as compared to that of the unsubstituted SWCNT-Pr1.

In the case of nanosecond laser pulse measurements, the third-order NLO response of porphyrin-functionalized carbon nanotubes derives primarily from three aspects: reverse saturable absorption (RSA) from porphyrins, nonlinear scattering (NLS) from SWCNTs, and the ET/PET between these components. SWCNTs have shown strong OL effects in the nanosecond regime due to the formation of new nonlinear scattering centers of ionized carbon microplasmas and solvent microbubbles [34,35]. In the present work, because all hybrid composites consist of SWCNTs from the same batch and each has highly efficient internal ET/PET processes indicated by the high fluorescence quenching yields all above 97%, it is likely that the RSA performance of the porphyrins is the most important determinant in modulating the overall NLO performance of the composites. Such RSA processes arise from the absorption of excited states and can be evaluated from the ratio k_a of the excited-state absorption cross-section (σ_{ex}) to the ground-state absorption cross-section (σ_0). k_a for Pr1, Pr2, and Pr3 in this work were calculated to be 1.90, 1.95, and 2.40, respectively. It can thus be seen that Pr2 with a CN substituent possesses a marginally greater RSA

ability as compared to that of the control Pr1, while the electron-donating DMA group affords Pr3 the highest σ_{ex}/σ_0 ratio and the strongest RSA performance, which is in good agreement with the enhanced OL effects discussed above. We believe that the increase in RSA upon introducing CN or DMA groups into porphyrins is largely responsible for optimizing the OL effects in the present SWCNT–Pr nanohybrids, and this may be a useful guideline for optimizing other hybridized optical limiters.

We also obtained the β values of the three new porphyrins and SWCNT–Pr1, SWCNT–Pr2 and SWCNT–Pr3 from numerically fitting the Z-scan curves obtained using an open-aperture configuration (Table 2). SWCNT–Pr3 showed the largest β value of 2.30×10^{-10} m/W of the three composites (in the case of SWCNT–Pr1 and SWCNT–Pr2, the corresponding values are 1.95×10^{-10} and 2.00×10^{-10} m/W, respectively). The Prs exhibit the same trend but with larger β values due to the NLA predominantly originating from RSA.

Table 2. NLO coefficients of the composites and Pr1-Pr3 in DMF at 532 nm.

Sample	I_0(J/cm^2)	T(%)	β ($\times 10^{-10}$m/W)	k_a
p-SWCNTs	0.54	68	1.30	−
SWCNT–Pr1	0.54	68	1.95	−
SWCNT–Pr2	0.54	68	2.00	−
SWCNT–Pr3	0.54	68	2.30	−
Pr1	0.54	68	6.10	1.90
Pr2	0.54	68	8.50	1.95
Pr3	0.54	68	10.0	2.40

4. Conclusion

Three novel porphyrin-covalently-functionalized SWCNTs (SWCNT–Pr1, SWCNT–Pr2, and SWCNT–Pr3) have been prepared with different organic substituents (H, CN, DMA) on the periphery of the porphyrins. The hybridization synthetic procedure involved initial alkyne attachment, de-protection, and finally azide-alkyne cycloaddition, forming a π-conjugated bridge of 4-*p*-phenylene-1,2,3-triazole which established an effective fluorescence quenching channel for possible ET/PET processes from porphyrins to SWCNTs, and with quenching yields above 97%. The covalent linkages were confirmed by multiple

techniques, including UV–vis, fluorescence, FTIR, and Raman spectroscopies, XPS, SEM, TEM, and TGA. The nonlinear transmittance tests revealed the superior OL properties of the novel composites over their individual components. More importantly, the RSA ability of the porphyrin components makes a major contribution to modulating the OL response of the composites, with the additional organic substituents (CN or DMA) affording a positive influence by increasing the σ_{ex}/σ_0 ratio and the RSA ability of the Pr precursors and thus the final OL performance of either Prs or SWCNT–Prs. In addition, in comparison with CN, the electron-donating DMA group has a more positive influence on the excited states of the porphyrins, and thus effectively enhances the RSA process and the global NLO performance of the SWCNT–Pr nanohybrids. This work contributes to the goal of rational design of better optoelectronic devices such as those in solar energy conversion and light limiting applications.

Acknowledgments

This research was financially supported by the National Natural Science Foundation of China (Nos. 51432006 and 51172100), the Ministry of Education and the State Administration of Foreign Experts Affairs for the 111 Project (No. B13025), the Ministry of Education of China for the Changjiang Innovation Research Team (No. IRT14R23), 100 Talents Program of CAS, and the Ministry of Science and Technology of China for International Science Linkages Program (2011DFG52970). M.G.H. and C.Z. thank the Australian Research Council for support.

Appendix A. Supplementary data

Supplementary materials (synthesis details of compound 1 and 2, Raman spectra of Pr2 at 532 and 785 nm, Zn 2p XPS spectra of SWCNT-Pr1 and SWCNT-Pr2, the open aperture Z-scan curve of blank DMF) are available online.

Notes

[1]M. F. Zhang and L. L. Fu contributed equally to this work.

References

[1] S.S. Babu, H. Möehwald, T. Nakanishi, Recent progress in morphology control of supramolecular fullerene assemblies and its applications, Chem. Soc. Rev. 39(11) (2010) 4021-4035.

[2] X.M. Sun, T. Chen, Z.B. Yang, H.S. Peng, The alignment of carbon nanotubes: an effective route to extend their excellent properties to macroscopic scale, Acc. Chem. Res. 46(2) (2013) 539-549.

[3] S. Stankovich, D.A. Dikin, G.H.B. Dommett, K.M. Kohlhaas, E.J. Zimney, E.A. Stach, R.D. Piner, S.T. Nguyen, R.S. Ruoff, Graphene-based composite materials, Nature 442 (2006) 282-286.

[4] A. Hirsch, Functionalization of single-walled carbon nanotubes, Angew. Chem. Int. Ed. 41(11) (2002) 1853-1859.

[5] M.C. Hersam, Progress towards monodisperse single-walled carbon nanotubes, Nat. Nanotech. 3(7) (2008) 387-394.

[6] Y.L. Zhao, J.F. Stoddart, Noncovalent functionalization of single-walled carbon nanotubes, Acc. Chem. Res. 42(8) (2009) 1161-1171.

[7] P. Singh, S. Campidelli, S. Giordani, D. Bonifazi, A. Biancoa, M. Prato, Organic functionalization and characterization of single-walled carbon nanotubes, Chem. Soc. Rev. 38(8) (2009) 2214-2230.

[8] X.F. Guo, Single-molecule electrical biosensors based on single-walled carbon nanotubes, Adv. Mater. 25(25) (2013) 3397-3408.

[9] Q. Cao, S. Han, Single-walled carbon nanotubes for high-performance electronics, Nanoscale 5(19) (2013) 8852-8863.

[10] S. Nanot, E.H. Hároz, J.H. Kim, R.H. Hauge, J. Kono, Optoelectronic properties of single-wall carbon nanotubes, Adv. Mater. 24(36) (2012) 4977-4994.

[11] H. Sharghi, S. Ebrahimpourmoghaddam, M.M. Doroodmand, Iron-doped single walled carbon nanotubes as an efficient and reusable heterogeneous catalyst for the synthesis of organophosphorus compounds under solvent-free condition, Tetrahedron 69(23) (2013) 4708-4724.

[12] F. Valentini, M. Carbone, G. Palleschi, Carbon nanostructured materials for applications in nano-medicine, cultural heritage, and electrochemical biosensors, Anal. Bioanal. Chem. 405(2) (2013) 451-465.

[13] R.L. McSweeney, T.W. Chamberlain, E.S. Davies, A.N. Khlobystov, Single-walled carbon nanotubes as nanoelectrode and nano-reactor to control the pathways of a redox reaction, Chem. Commun. 50(92) (2014) 14338-14340.

[14] M.N. Ding, D.C. Sorescu, A. Star, Photoinduced charge transfer and acetone sensitivity of single walled carbon nanotube-titanium dioxide hybrids, J. Am. Chem. Soc. 135(24) (2013) 9015-9022.

[15] H. Kitano, K. Tachimoto, Y. Anraku, Functionalization of single-walled carbon nanotube by the covalent modification with polymer chains, J. Colloid. Interf. Sci. 306(1) (2007) 28-33.

[16] J. Luan, P.X. Hou, C. Liu, C. Shi, G.X. Li, H.M. Cheng, Efficient adsorption of organic dyes on a flexible single-wall carbon nanotube film, J. Mater. Chem. A 4(4) (2016) 1191-1194.

[17] F.Y. Cheng, J. Zhu, A. Adronov, Supramolecular functionalization of single-walled carbon nanotubes with triply fused porphyrin dimers: a study of structure property relationships, Chem. Mater. 23(13) (2011) 3188-3194.

[18] P. d'Ambrosio, M. Carchesio, N. d'Alessandro, G. de la Torre, T. Torres, Linking Pd(II) and Ru(II) phthalocyanines to single-walled carbon nanotubes, Dalton. Trans. 43(20) (2014) 7473-7479.

[19] M.O. Senge, M. Davis, Porphyrin (porphine)-A neglected parent compound with potential, J. Porphyr. Phthalocya. 14(7) (2010) 557-567.

[20] M.O. Senge, M. Fazekas, E.G.A. Notaras, W.J. Blau, M. Zawadzka, O.B. Locos, E.M.N. Mhuircheartaigh, Nonlinear optical properties of porphyrins, Adv. Mater. 19(19) (2007) 2737-2774.

[21] S.M.B. Costa, S.M. Andrade, D.M. Togashi, P.M.R. Paulo, C.A.T. Laia, M.I. Viseu, A.M.G. da Silva, Optical spectroscopy and photochemistry of porphyrins and phthalocyanines, J. Porphyr. Phthalocya. 13(4&5) (2009) 509-517.

[22] R. Paolesse, S. Nardis, D. Monti, M. Stefanelli, C.D. Natale, Porphyrinoids for chemical sensor applications, Chem. Rev. 117(4) (2017) 2517-2583.

[23] M. Urbani, M. Grätzel, M.K. Nazeeruddin, T. Torres, Meso-substituted porphyrins for dye-sensitized solar cells, Chem. Rev. 114(24) (2014) 12330-12396.

[24] K.S. Suslick, N.A. Rakow, M.E. Kosal, J.H. Chou, The materials chemistry of porphyrins and metalloporphyrins, J. Porphyr. Phthalocya. 4(4) (2000) 407-413.

[25] J.S. Lindsey, Synthetic routes to meso-patterned porphyrins, Acc. Chem. Res. 43(2) (2010) 300-311.

[26] A.S.D. Sandanayaka, O. Ito, Photoinduced electron transfer in supramolecules composed of porphyrin/phthalocyanine and nanocarbon materials, J. Porphyr. Phthalocya. 13(10) (2009) 1017-1033.

[27] F. D'Souza, O. Ito, Supramolecular donor-acceptor hybrids of porphyrins/phthalocyanines with fullerenes/carbon nanotubes: electron transfer, sensing, switching, and catalytic applications, Chem. Commun. 33 (2009) 4913-4928.

[28] D.M. Guldi, G.M.A. Rahman, M. Prato, N. Jux, S.H. Qin, W. Ford, Single-wall carbon nanotubes as integrative building blocks for solar-energy conversion, Angew. Chem. Int. Ed. 117(13) (2005) 2051-2054.

[29] X.L. Zhang, Z.B. Liu, X. Zhao, X.Q. Yan, X.C. Li, J.G. Tian, Optical limiting effect and ultrafast saturable absorption in a solid PMMA composite containing porphyrin-covalently functionalized multi-walled carbon nanotubes, Opt. Express. 21(21) (2013) 25277-25284.

[30] Z.B. Liu, J.G. Tian, Z. Guo, D.M. Ren, J.Y. Zheng, Y.S. Chen, Enhanced optical limiting effects in porphyrin-covalently functionalized single-walled carbon

nanotubes, Adv. Mater. 20(3) (2008) 511-515.

[31] E.M.N. Mhuircheartaigh, S. Giordani, W.J. Blau, Linear and nonlinear optical characterization of a tetraphenylporphyrin-carbon nanotube composite system, J. Phys. Chem. B 110(46) (2006) 23136-23141.

[32] J. Gupta, C. Vijayan, S.K. Maurya, D. Goswami, Efficient ultrafast optical limiting using single walled carbon nanotubes functionalized noncovalently with free base and metalloporphyrins, J. Appl. Phys. 109 (2011) 113101-113106.

[33] F.Y. Cheng, A. Adronov, Suzuki coupling reactions for the surface functionalization of single-walled carbon nanotubes, Chem. Mater. 18(23) (2006) 5389-5391.

[34] Z. Guo, F. Du, D.M. Ren, Y.S. Chen, J.Y. Zheng, J.G. Tian, Covalently porphyrin-functionalized single-walled carbon nanotubes: a novel photoactive and optical limiting donor-acceptor nanohybrid, J. Mater. Chem. 16(29) (2006) 3021-3030.

[35] C. Ehlia, S. Campidellib, F.G. Brunettib, M. Prato, D.M. Guldi, Single-wall carbon nanotube porphyrin nanoconjugates, J. Porphyr. Phthalocya. 11(6) (2007) 442-447.

[36] H.Y. Zhao, Y.Z. Zhu, C. Chen, L. He, J.Y. Zheng, Synthesis, characterization, and photophysical properties of covalent-linked ferrocene-porphyrin-single-walled carbon nanotube triad hybrid, Carbon 50(13) (2012) 4894-4902.

[37] S.K. Das, A.S.D. Sandanayaka, N.K. Subbaiyan, M.E. Zandler, O. Ito, F. D'Souza, Functionalization of diameter sorted semi-conductive SWCNTs with photosensitizing porphyrins: syntheses and photoinduced electron transfer, Chem. Eur. J. 18(36) (2012) 11388-11398.

[38] S.K. Kim, S. Jeon, Improved electrocatalytic effect of carbon nanomaterials by covalently anchoring with CoTAPP via diazonium salt reactions, Electrochem. Commun. 22(2012) 141-144.

[39] K.S. Suslick, C.T. Chen, G.R. Meredith, L.T. Cheng, Push-pull porphyrins as nonlinear optical materials, J. Am. Chem. Soc. 114(17) (1992) 6928-6930.

[40] Kc. Ogawa, T.Q. Zhang, K. Yoshihara, Y. Kobuke, Large third-order optical nonlinearity of self-assembled porphyrin oligomers, J. Am. Chem. Soc. 124(1) (2002) 22-23.

[41] X.D. Feng, M.O. Senge, An efficient synthesis of highly functionalized asymmetric porphyrins with organolithium reagents, J. Chem. Soc., Perkin Trans. 1(9) (2001) 1030-1038.

[42] X.D. Feng, I. Bischoff, M.O. Senge, Mechanistic studies on the nucleophilic reaction of porphyrins with organolithium reagents, J. Org. Chem. 66(26) (2001) 8693-8700.

[43] M. Sheik-Bahae, A.A. Said, T.H. Wei, D.J. Hagan, E.W. Van Stryland, Sensitive measurement of optical nonlinearities using a single beam, IEEE. J. Quant. Electron. 26 (1990) 760-769.

[44] K. Manabe, Palladium catalysts for cross-coupling reaction, Catalysts 5(1) (2015)

38-39.

[45] J.A. Fagan, C.Y. Khripin, M. Zheng, Isolation of specific small-diameter single-wall carbon nanotube species via aqueous two-phase extraction, Adv. Mater. 26(18) (2014) 2800-2804.

[46] A. Köhn, C. Hättig, On the nature of the low-lying singlet states of 4-(dimethyl-amino)benzonitrile, J. Am. Chem. Soc. 126(23) (2004) 7399-7410.

[47] G. Ramakrishna, A.K. Singh, H.N. Ghosh, Effect of molecular structure on interfacial electron transfer dynamics of 7-N,N-dimethyl coumarin 4-aetic acid (DMACA) and 7-hydroxy coumarin 4-acetic acid (HCA) sensitized TiO2 and ZrO2 nanoparticles, J. Phys. Chem. B 108(33) (2004) 12489-12496.

[48] Y.S. Wu, Y.G. Zhen, Z.H. Wang, H.B. Fu, Donor-linked di(perylene bisimide)s: arrays exhibiting fast electron transfer for photosynthesis mimics, J. Phys. Chem. A 117(8) (2013) 1712-1720.

[49] A.S.D. Sandanayaka, R. Chitta, N.K. Subbaiyan, L. D'Souza, O. Ito, F. D'Souza, Photoinduced charge separation in ion-paired porphyrin-single-wall carbon nanotube donor-acceptor hybrids, J. Phys. Chem. C 113(30) (2009) 13425-13432.

[50] C.W. Tornøe, C. Christensen, M. Meldal, Peptidotriazoles on solid phase: [1,2,3]-triazoles by regiospecific copper(i)-catalyzed 1,3-dipolar cycloadditions of terminal alkynes to azides, J. Org. Chem. 67(9) (2002) 3057-3064.

[51] A.J. Wang, L.L. Long, W. Zhao, Y.L. Song, M.G. Humphrey, M.P. Cifuentes, X.Z. Wu, Y.S. Fu, D.D. Zhang, X.F. Li, C. Zhang, Increased optical nonlinearities of graphene nanohybrids covalently functionalized by axially-coordinated porphyrins, Carbon 53 (2013) 327-338.

[52] J. Raushel, V.V. Fokin, Efficient synthesis of 1-sulfonyl-1,2,3-triazoles, Org. Lett. 12(21) (2010) 4952-4955.

[53] N. Noshiranzadeh, M. Emami, R. Bikas, A. Kozakiewicz, Green click synthesis of β-hydroxy-1,2,3-triazoles in water in the presence of Cu(II)-azide catalyst: a new function for Cu(II)-azide complexes, New. J. Chem. 41(7) (2017) 2658-2667.

[54] S. Eyley, S. Shariki, S.E.C. Dale, S. Bending, F. Marken, W. Thielemans, Ferrocene-decorated nanocrystalline cellulose with charge carrier mobility, Langmuir 28(16) (2012) 6514-6519.

[55] Y. Miyata, K. Mizuno, H. Kataura, Purity and defect characterization of single-walled carbon nanotubes using raman spectroscopy, J. Nanomater. 2011 (2011) 786763 1-7.

[56] A.J. Wang, J.B. Song, Z.P. Huang, Y.L. Song, W. Yu, H.L. Dong, W.P. Hu, M.P. Cifuentes, M.G. Humphrey, L. Zhang, J.D. Shao, C. Zhang, Multi-walled carbon nanotubes covalently functionalized by axially coordinated metal-porphyrins: facile syntheses and temporally dependent optical performance, Nano. Res. 9(2) (2016) 458-472.

[57] V.M. Irurzun, M.P. Ruiz, D.E. Resasco, Raman intensity measurements of single-walled carbon nanotube suspensions as a quantitative technique to assess

purity, Carbon 48 (2010) 2873-2881.

[58] V. Georgakilas, A. Bourlinos, D. Gournis, T. Tsoufis, C. Trapalis, A. Mateo-Alonso, M. Prato, Multipurpose organically modified carbon nanotubes: from functionalization to nanotube composites, J. Am. Chem. Soc. 130(27) (2008) 8733-8740.

[59] A.J. Wang, Y. Fang, L.L. Long, Y.L. Song, W. Yu, W. Zhao, M.P. Cifuentes, M.G. Humphrey, C. Zhang, Facile synthesis and enhanced nonlinear optical properties of porphyrin-functionalized multi-walled carbon nanotubes, Chem. Eur. J. 19(42) (2013) 14159-14170.

[60] S. Campidelli, B. Ballesteros, A. Filoramo, D.D. Díaz, G. de la Torre, T. Torres, G.M.A. Rahman, C. Ehli, D. Kiessling, F. Werner, V. Sgobba, D.M. Guldi, C. Cioffi, M. Prato, J. Bourgoin, Facile decoration of functionalized single-wall carbon nanotubes with phthalocyanines via “click chemistry”, J. Am. Chem. Soc. 130(34) (2008) 11503-11509.

[61] S. Fedeli, A. Brandi, L. Venturini, P. Chiarugi, E. Giannoni, P. Paoli, D. Corti, G. Giambastiani, G. Tuci, S. Cicchi, the ‘click-on-tube’ approach for the production of efficient drug carriers based on oxidized multi-walled carbon nanotubes, J. Mater. Chem. B 131(42) (2009) 15394-15402.

[62] T. Palacin, H.L. Khanh, B. Jousselme, P. Jegou, A. Filoramo, C. Ehli, D.M. Guldi, S. Campidelli, Efficient functionalization of carbon nanotubes with porphyrin dendrons via click chemistry, J. Am. Chem. Soc. 131 (2009) 15394-15402.

[63] V. Spampinato, G. Ceccone, S. Giordani, Surface analysis of zinc-porphyrin functionalized carbon nano-onions, Biointerphases 10(1) (2015) 019006 1-8.

[64] A. Bensghaïer, Z. Salmi, B.L. Droumaguet, A. Mekki, A.A. Mohamed, M. Beji, M.M. Chehimib, Diazonium interface chemistry and click polymerization: a novel route for carbon nanotube-polytriazole nanocomposites, Surf. Interf. Anal. 48 (2016) 509-513.

[65] H.Y. Zhao, Y.Z. Zhu, L. He, J.Y. Zheng, Synthesis, characterization, and photophysical properties of covalent-linked ferrocene-porphyrin-single-walled carbon nanotube triad hybrid, Carbon 50(13) (2012) 4894-4902.

[66] J. Wang, Y. Chen, R.H. Li, H.X. Dong, Y.F. Ju, J. He, J.T. Fan, K.P. Wang, K.S. Liao, L. Zhang, S.A. Curran, W.J. Blau, Graphene and carbon nanotube polymer composites for laser protection, J. Inorg. Organomet. P 21(4) (2011) 736-746.

[67] X.M. Gu, W. Qi, X.Z. Xu, Z.H. Sun, L.Y. Zhang, W. Liu, D.S. Su, Covalently functionalized carbon nanotube supported Pd nanoparticles for catalytic reduction of 4-nitrophenol, Nanoscale 6(12) (2014) 6609-6616.

[68] A.M. Díez-Pascual, M. Naffakh, Grafting of an aminated poly(phenylene sulphide) derivative to functionalized single-walled carbon nanotubes, Carbon 50(3) (2012) 857-868.

[69] M.L. Wang, K.J. Yu, K. Qian, In situ synthesis of carbon nanotubes/graphene nanoplatelets hybrid materials with excellent mechanical performance, Nano 10(4) (2015) 1550055.

[70] A.J. Wang, J.B. Song, D. Jia, W. Yu, L.L. Long, Y.L. Song, M.P. Cifuentes, M.G. Humphrey, L. Zhang, J.D. Shao, C. Zhang, Functionalization of reduced graphene oxide with axially-coordinated metal-porphyrins: facile syntheses and temporally-dependent nonlinear optical properties, Inorg. Chem. Front. 3(2) (2016) 296-305.

[71] A.J. Wang, Y. Fang, W. Yu, L.L. Long, Y.L. Song, W. Zhao, M.P. Cifuentes, M. G. Humphrey, C. Zhang, Allyloxyporphyrin-functionalized multiwalled carbon nanotubes: synthesis by radical polymerization and enhanced optical-limiting properties, Chem. Asian. J. 9(2) 2014 639-648.

[72] L.M. Arellano, M. Barrejón, H.B. Gobeze, M.J. Gómez-Escalonilla, J.L.G. Fierro, F. D'Souza, F. Langa, Charge stabilizing tris(triphenylamine)-zinc porphyrin-carbon nanotube hybrids: synthesis, characterization and excited state charge transfer studies, Nanoscale 9(22) (2017) 7551-7558.

[73] H. van der Salm, P. Wagner, K. Wagner, D.L. Officer, G.G. Wallace, K.C. Gordon, Flexible tuning of unsaturated beta-substituents on Zn porphyrins: a synthetic, spectroscopic and computational study, Chem. Eur. J. 21(44) (2015) 15622-15632.

[74] J.C.P. Mayer, A.C. Sauer, B.A. Iglesias, T.V. Acunha, D.F. Back, O.E.D. Rodrigues, L. Dornelles, Ferrocenylethenyl-substituted 1,3,4-oxadiazolyl-1,2,4-oxadiazoles: synthesis, characterization and DNA-binding assays, J. Organomet. Chem. 841 (2017) 1-11.

[75] N. Aratani, D. Kim, A. Osuka, pi-Conjugation enlargement toward the creation of multi-porphyrinic systems with large two-photon absorption properties, Chem. Asian. J. 4(8) (2009) 1172-1182.

[76] G.H. Ao, X.M. Qian, Z.G. Xiao, Z.G. Li, Z.Q. Nie, Y.X. Wang, X.R. Zhang, Y.L. Song, Modulation of internal conversion rate and nonlinear absorption in meso-tetraphenylporphyrins by donor/acceptor substitutes, Opt. Mater. 46 (2015) 578-584.